Short communication

GMR biosensor arrays: Correction techniques for reproducibility and enhanced sensitivity

D.A. Hall [a], R.S. Gaster [b,c], S.J. Osterfeld [d], B. Murmann [a], S.X. Wang [a,e,*]

[a] Department of Electrical Engineering, Stanford University, Stanford, CA 94305, USA
[b] Department of Bioengineering, Stanford University, Stanford, CA 94305, USA
[c] Medical Scientist Training Program, Stanford University School of Medicine, Stanford, CA 94305, USA
[d] MagArray, Inc., Sunnyvale, CA 94089, USA
[e] Department of Materials Science and Engineering, Stanford University, Stanford, CA 94305, USA

ARTICLE INFO

ABSTRACT

Giant magnetoresistive biosensors possess great potential in biomedical applications for quantitatively detecting magnetically tagged biomolecules. Magnetic sensing does not suffer from the high background levels found in optical sensing modalities such as the enzyme linked immunosorbent assay translating into a technology with higher sensitivity. However, to reveal the full potential of these sensors and compensate for non-idealities such as temperature dependence, digital correction and calibration techniques are not only useful but imperative. Using these calibration techniques to correct for process variations and dynamic changes in the sensing environment (such as temperature and magnetic field), we are able to obtain extremely sensitive and, more importantly, reproducible results for quantifiable biomolecular reorganization. The reproducibility of the system was improved by over $3\times$ using digital correction techniques and the sensors are made temperature independent by using a novel background correction technique.

1. Introduction

Giant magnetoresistive (GMR) biosensors are capable of highly sensitive detection of proteins and nucleic acids (Baselt et al., 1998; Graham et al., 2004; de Boer et al., 2007; Xu et al., 2008; Osterfeld et al., 2008). Furthermore, these sensors can be arrayed to monitor large panels of proteins simultaneously (Osterfeld et al., 2008). For protein detection, a capture antibody is immobilized on the surface of an individually addressable sensor to selectively capture the target analyte. The high specificity of the bioassay is achieved from the selectivity of the capture antibody. Subsequently, a detection antibody labeled with a magnetic nanoparticle (MNP) binds to the analyte. The local magnetic field above the sensor is altered by the presence of these surface bound MNPs. Detecting biological molecules labeled with MNP tags using GMR spin-valve sensors requires monitoring miniscule resistance changes, as small as a few micro-ohms, in a dynamic environment where temperature changes up to 30 °C are possible. The change in magnetoresistance (MR) of the spin-valve biosensor is proportional to the number of surface bound MNPs and calibration curves are used to translate this change in MR into an analyte concentration. However, process variation causes the resistance, MR, and the transfer curves of each sensor to deviate significantly from the nominal specification. As the number of sensors in the array increases, these statistical variations become more noticeable and interfere with the objective to obtain reproducible results. Reproducible and sensitive operation necessitates correction algorithms and techniques to account for process variations found in the sensors, front-end electronics, temperature induced signals, and magnetic field non-uniformity.

2. Materials and methods

The biosensor array used in this work is composed of an 8×8 grid of individually addressable GMR spin-valve sensors. A double modulation scheme modulates the signal from the MNPs away from the flicker noise of the sensor and the flicker noise of the electronics (de Boer et al., 2007; Han et al., 2007). By modulating the magnetic field (at frequency f_f) and the voltage applied to the sensor (at frequency f_c), the sensor appears like a mixer. The output spectrum contains a carrier tone (CT) at f_c and two side tones (ST) at $f_c - f_f$ and $f_c + f_f$ (Supplementary Fig. 1). For brevity, the carrier tone will henceforth be referred to simply as CT and the side tones ST. In situations where it is necessary to differentiate the lower (at $f_c - f_f$) and upper (at $f_c + f_f$) side tones, they will be referred to as the

* Corresponding author at: Department of Materials Science and Engineering, Stanford University, 476 Lomita Mall, McCullough Bldg. R351, Stanford, CA 94305, USA.

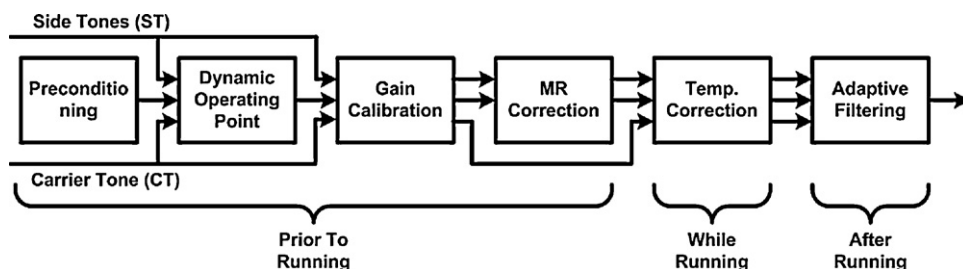E-mail address: sxwang@stanford.edu (S.X. Wang).

Fig. 1. Overview of the corrections and order in which they are applied.

LT and UT respectively. The modulated magnetic field, referred to as the tickling field, is applied along the hard axis of the sensor's free layer. The signal path consists of a GMR spin-valve sensor followed by a transimpedance amplifier (TIA) and an instrumentation amplifier (IA) used to suppress the carrier and provide additional gain (Supplementary Fig. 2). When referring to the CT, it is assumed that the carrier tone has been reconstructed in software after digitization to restore the portion of the signal suppressed by the carrier suppression circuit. A detailed description of the electronics can be found elsewhere (Hall et al., 2009a).

Fig. 1 shows an overview of the sensor signal acquisition and correction techniques presented in this paper and the order in which they are applied. The process includes three major steps: (1) prior to running a bioassay experiment, the procedure includes preconditioning (Supplementary Section 1), establishing the dynamic operating point, gain calibration (Supplementary Section 2), and MR correction. (2) While the bioassay is running, CT and ST signals are acquired, and the temperature correction algorithm is applied in real-time to compensate for changes in the sensing environment. (3) Lastly, an adaptive filter is applied after the bioassay is completed to decrease the noise and improve the signal to noise ratio. The following sections will describe these techniques in detail followed by demonstration of their performance in practice.

2.1. Dynamic operating point

With the double modulation scheme, the MR of each sensor is computed from the amplitude of the CT and the ST as shown in Eq. (1) (see Supplementary Section 3 for a derivation). This equation provides a rapid method to compute the MR under a variety of different operating conditions and optimally sets the operating point of the sensor by adjusting the amplitude of the tickling field. Increasing the amplitude of the tickling field increases the MR, until the sensor reaches the saturation point. However, as the ticking field amplitude increases, the sensitivity (slope of the transfer curve) diminishes. These counteracting effects create an optimum operating point which depends on both the sensor and the magnetic tags. Previously, it was found that a tickling field of 25 Oe was optimal for the 750 nm sensors and MACS superparamagnetic nanoparticles used in these experiments (Hall et al., 2009a):

$$MR = \frac{CT + 2ST}{CT - 2ST} - 1 \qquad (1)$$

Global process variations as well as shifts in the nominal resistance and/or MR of the sensor, make operating at a set tickling field amplitude unreliable. Rather than applying a fixed field, we target a specific value of MR to improve the reproducibility of the experiments. By applying several different magnetic fields and calculating the MR at each field (using Eq. (1)), the target tickling field is calculated by interpolating the measured values. This feedback also desensitizes the system to variability (such as aging or tem-

perature dependence) in the power amplifier and electromagnet. Dynamically setting the operating point by adjusting the tickling field maximizes the sensitivity of the sensor array and improves the reproducibility despite process variations.

2.2. MR calibration

Magnetic field variations exist across the sensor array and require correction because the change in MR over time is used to infer the number of surface bound MNPs. Both the magnetic moment of the superparamagnetic tag and the operating point on the transfer curve are determined by the magnetic tickling field making the system very sensitive to field variations across the sensor array. Without correction, a sensor in the center of the array and one on the edge with the same number of surface bound MNPs would produce unequal results, hindering the utility and degrading the sensitivity of the system. Furthermore, the sensor to sensor variation of the MR is indistinguishable from the field non-uniformity, further compounding the problem. Here, we present two different solutions to correct for this effect.

By changing the amplitude of the tickling field, effectively applying a step, the resulting change in MR is observed (Eq. (1)). Measuring the MR in this fashion is not possible if the sensor is in a bridge configuration since both sensors will experience the same change in magnetic field and cancel. An MR calibration coefficient is calculated for each sensor from the inverse of the MR change over the median MR change of the entire array. This coefficient is then multiplied by both the ST amplitudes. An obvious extension from this one point calibration is to repeat this process for many different ticking field amplitudes, essentially measuring the transfer curve of each sensor. Fortunately, in biosensing applications, the change in the local magnetic field due to the MNPs is sufficiently small that it is unnecessary to measure the entire transfer curve as a linear interpolation is adequate.

An even more straightforward approach utilizes the absolute amplitude of the STs rather than the response due to magnetic field changes. This method has the advantage that the effectiveness of the calibration can be verified by applying one or more magnetic field steps and observing the uniformity of the responses. This method is similar to an offset calibration and assumes that the transfer curves are all identical, just operating at a different point due to the field variations. Calibrating for the non-uniformity in the magnetic tickling field is the most important step in achieving high reproducibility, particularly in large arrays. Additionally, this calibration step (either method) quickly identifies unresponsive sensors which are marked as defective decreasing the false negative rate in a bioassay.

2.3. Temperature correction

Spin-valves, like most sensors, exhibit temperature dependence and have fairly large temperature coefficients (TC), hundreds to

thousands of PPM/°C for both the resistive and the magnetoresistive components (Daughton and Chen, 1993; Lenssen et al., 2000). Even small temperature fluctuations can easily induce responses larger than the signal due to the magnetic tags. Here we present a novel solution that does not require the need for precise temperature regulation (Wang et al., 2009; Han et al., 2007; Almeida et al., 2006) or the need to modulate the magnetic bias field (applied orthogonal to the tickling field) (Han et al., 2007). The crux of our approach is to use the sensor to sense the relative temperature change and literally correct itself. Importantly, this correction can be applied in the background without taking the sensor offline (Hall et al., 2009b).

As described earlier, the double modulation scheme separates the resistive and magnetoresistive components of the sensor by modulating them to different frequencies. Eq. (2) shows the output of a GMR sensor using the double modulation scheme where the resistance of the sensor at the operating point is denoted by R_0 and the magnetoresistive component is ΔR_0 with a voltage V being applied to the sensor. While presented here for a voltage excitation, the same approach (and many of the results) hold for a current excitation as well:

$$I_{\mathrm{GMR}}(t) = \frac{V \cos(2\pi f_c t)}{R_0(1 + \alpha \Delta T) + ((\Delta R/2(1 + \beta \Delta T))\cos(2\pi f_f t)} \quad (2)$$

The non-magnetoresistive portion of the sensor has a TC, α, and the magnetoresistive portion has a TC, β, both of which are strongly dependent on the materials used to manufacture the sensor and the subsequent device fabrication steps. The relationship between α and β is however independent of temperature. Expanding out Eq. (2) and isolating the different tones based on the frequency, we derived approximate expressions for each of the tones (Eqs. (3) and (4)) where $\bar{V}$ is the RMS voltage applied to the sensor (see Supplementary Section 4 for the derivation):

$$\overline{I_{\mathrm{CT}}} \approx \frac{\bar{V}}{R_0}(1 - \alpha \Delta T) \quad (3)$$

$$\overline{I_{\mathrm{ST}}} \approx \frac{\bar{V} \Delta R_0}{4R_0^2}(1 + (\beta - 2\alpha)\Delta T) \quad (4)$$

The relationship between α and β is determined empirically by intentionally inducing a temperature change at the sensor and observing the response of the CT and ST (Fig. 2a and b). After 2.5 min of observing a baseline signal, a cold solution was added directly on top of the sensors. The sensors initially rise very quickly and then slowly decay as the temperature of the solution equilibrates to room temperature. Interestingly, both the CT and ST spike up despite the opposite signs of the TCs for the resistive and magnetoresistive components (α is usually positive and β is almost always negative). However, this is easily explained because current biochip reader does not keep track of phase information. Since only the magnitude of the signals are acquired, there is a negative sign that gets dropped causing the ST to peak up (instead of down). The relationship between the TCs is calculated by relating the normalized tone values to their initial value (Eqs. (5) and (6)) and plotting them against each other (Fig. 2c):

$$\frac{\overline{I_{\mathrm{CT}}}(t)}{\overline{I_{\mathrm{CT}}}(0)} - 1 = \frac{(\bar{V}/R_0)(1 - \alpha \Delta T)}{\bar{V}/R_0} - 1 = -\alpha \Delta T \quad (5)$$

$$\frac{\overline{I_{\mathrm{ST}}}(t)}{\overline{I_{\mathrm{ST}}}(0)} - 1 = \frac{(\bar{V} \Delta R_0/4R_0^2)(1 + (\beta - 2\alpha)\Delta T)}{\bar{V} \Delta R_0/4R_0^2} - 1 = (\beta - 2\alpha)\Delta T \quad (6)$$

Typically a first order linear fit is sufficient to relate the temperature coefficients but a higher order fitting equation can be used to account for higher order temperature dependence. We define κ to represent the relationship between the temperature coefficients and the correction factor (CF) as shown in Eq. (7). The correction

factor utilizes the carrier tone to measure the relative change in temperature and the relationship between the temperature coefficients (κ) to invert the temperate effect on the side tones. Lastly, the side tone becomes temperature independent by multiplying the measured side tone amplitude by the correction factor. This technique is particularly effective because the relative temperate change is sensed by the same sensor it is applied to, making it useful even in the presence of temperature gradients across the sensor array:

$$CF = \frac{1}{1 + \kappa((\overline{I_{\mathrm{CT}}}(t))/\overline{I_{\mathrm{CT}}}(0)) - 1)} \quad (7)$$

2.4. Adaptive filtering

Replica copies of the side tone are created at the sensor (LT and UT) with the double modulation scheme and processed by the subsequent electronics. In the absence of noise and distortion, these signals would be identical. Realistically, however, they are both corrupted by noise, the exact characteristics of which are unknown prior to running a bioassay experiment. Averaging the two side tones is a simple approach to improving the signal to noise ratio (SNR) by $\sqrt{2}$. However, a more elegant solution is to use an adaptive filter which improves the SNR by N where N is the number of inputs (two in this case). Similar filters have been used in wireless communications where multiple time delayed signals are received (Ferrara and Widrow, 1981). The adaptive filter uses one of the two side tones to learn the optimal coefficients and the other is passed through the tuned filter which is implemented with a finite impulse response (FIR) filter. The coefficients of the filter are computed based on the least mean squares (LMS) algorithm to minimize the noise (Haykin and Widrow, 2003). This method of adaptive filtering is very effective at removing the uncorrelated noise in the side tones.

3. Results and discussion

To illustrate the effectiveness of the MR correction, Supplementary Fig. 3a and b shows the results before and after applying the absolute amplitude MR correction algorithm (the second method presented). The sensors were subjected to a 1 Oe change in the magnetic tickling field to simulate the effect of surface bound magnetic tags. Without the correction, the average response was 179 μV with a standard deviation of 6.1 μV. The average changed only slightly with the corrections enabled but the standard deviation was reduced 5-fold. Furthermore, even the outlier sensors with substantially higher responses were properly corrected. These sensors were located at the outermost edge of the array and had a slightly higher MR resulting in the larger uncorrected response. Furthermore, the MR correction algorithm is effective for many different field steps in the application range (Supplementary Fig. 3c and d). The results clearly demonstrate the effectiveness of the MR correction technique.

The temperature correction is a vital component to the biochip reader, particularly when looking at very low analyte concentrations where the binding signal is only a few microvolts (micro-ohms change in resistance or tens of PPM change in the MR) and the temperature induced signal can be tens of tens of microvolts or more. To demonstrate the effectiveness of the correction algorithm, we placed fluid of different temperatures directly on the sensors and observed the temperature induced signal. The fluid was cooled or heated to a known temperature (Fig. 2d) and placed on the sensor array which was being monitored in real-time. Without temperature correction, the signals peaked up (or down depending on if the solution was warmer or colder than room temperature) and then exponentially decayed back to the
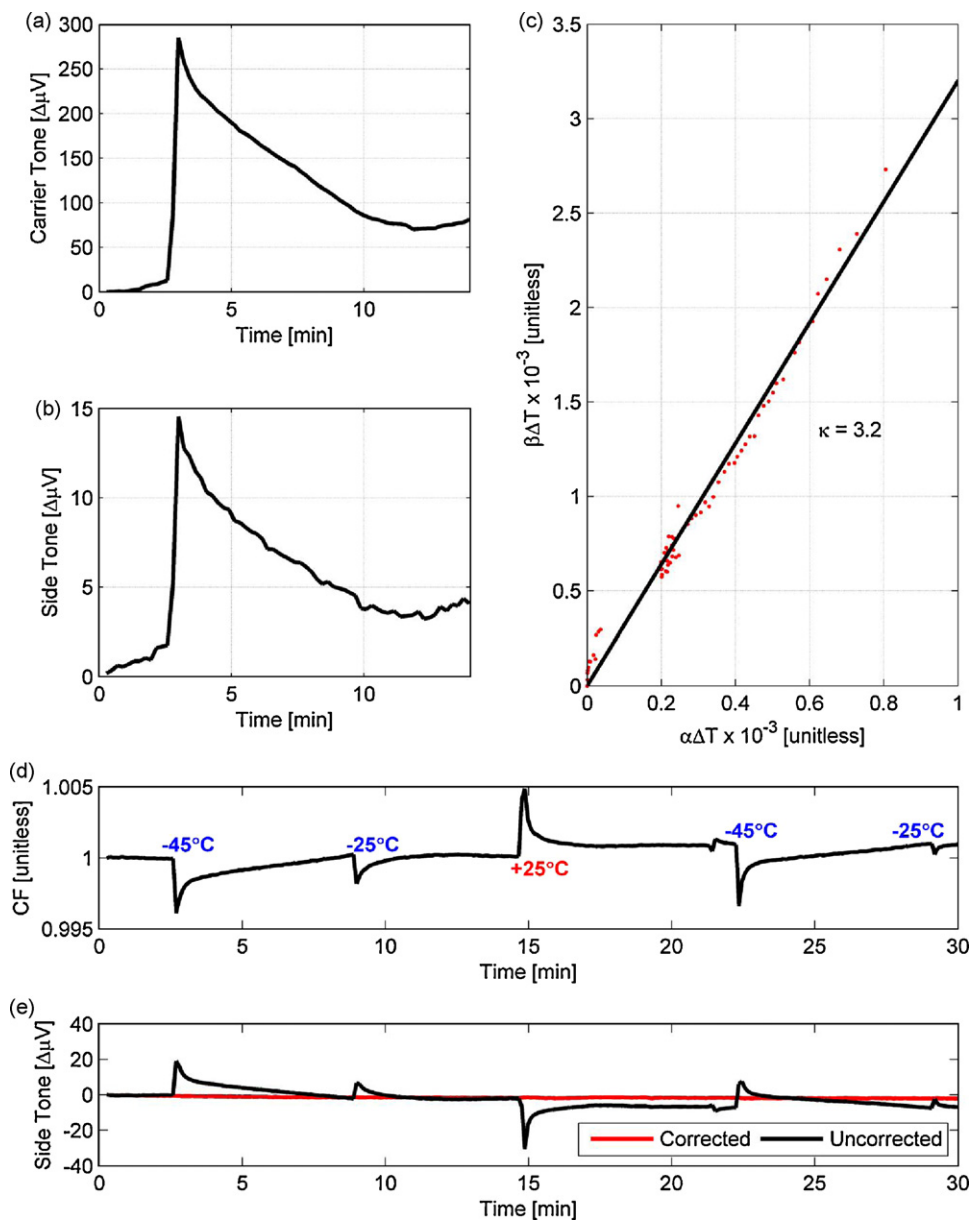
Fig. 2. Change in carrier tone (a) and side tone (b) with the addition of a solution 20 °C below room temperature. The points from the test are plotted against each other (c) to relate the temperature coefficients. (d) Correction factor (CF) annotated with the relative difference between the solution and room temperature. (e) Uncorrected real-time sensor response and corrected response.

nominal value (Fig. 2e). This response was due to the equilibration of the solution towards room temperature. Applying the temperature correction (Fig. 2e) removes the strong temperature dependence of the sensors equally well for both cold and hot solutions and is applied in real-time without taking the sensor offline.

When measuring low concentrations of biomolecules, the SNR of the signal becomes increasingly important. For one of our analytes, the lowest concentration we can quantifiably and reproducibly differentiate from the non-specific binding (negative control) is 5 fM without biological amplification. At this concentration, the SNR is only 8, making it difficult to determine the saturated amplitude. To demonstrate the effectiveness of the adaptive filter on a different analyte that we are currently optimizing, Supplementary Fig. 4a shows the lower and upper side tones of a protein assay with a concentration of 125 fM. The SNR prior to using the filter is just over 15 and it is difficult to determine the saturated

amplitude of the binding curve due to the noise. Depending on what portion of the curve is used, the value could be anywhere from 4.8 to 6.2 μV. After the adaptive filter (Supplementary Fig. 4b), the SNR has improved to over 30 and it is straightforward to determine the signal amplitude and correspondingly the analyte concentration from a calibration curve.

Lastly, the reproducibility with all of the correction techniques enabled is demonstrated by monitoring the simulated response of MNPs across many different wafers of sensors. For this study, 32 dies (from five wafers) each containing 64 sensors were exposed to a 0.5 Oe change in the tickling field (Fig. 3a and b). For each of the dies, the response is grouped by the sensor location (sensor 1 is in the top left and 64 is in the lower right) to prove that there is no systematic offset but rather the more than 2000 data points are dispersed randomly. The average response before and after corrections remains the same (103.40 and 103.44 μV) but the standard deviation has been reduced from 3 to 0.87 μV, a 3.4-
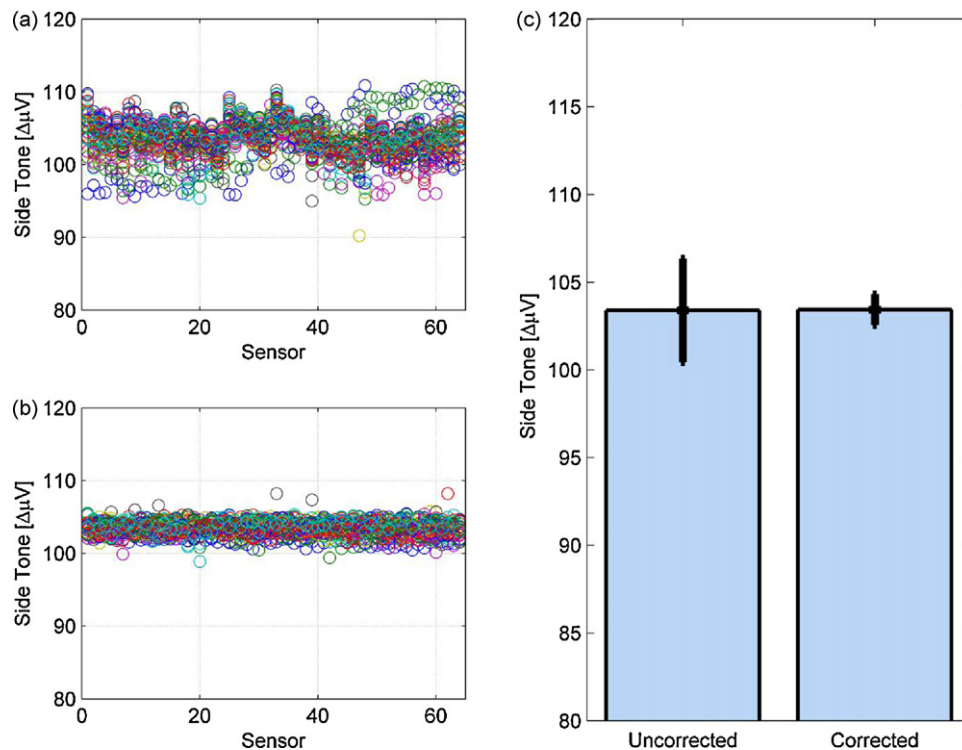
Fig. 3. (a) MR step amplitude without any corrections applied. (b) Data from (a) with gain correction and MR correction applied. (c) Average and standard deviation before and after corrections.

fold reduction. Fig. 3c summarizes the results, collected over many months, unequivocally showing the long-term reproducibility of the system utilizing the correction techniques presented in this paper.

4. Conclusion

Through calibration and correction, the sensitivity and reproducibility of GMR biosensors can be greatly improved. The correction techniques described in this paper are an important tool that helped our research group enhance the limit of detection in our protein assays by over three orders of magnitude. The robustness of the system was greatly improved by the temperature correction algorithm without requiring any form of temperature regulation or control. The techniques presented here are scalable to even larger arrays of GMR sensors. Furthermore, we are routinely able to reproduce the results, allowing protein concentration calibration curves to be used for several months and extensive preclinical or clinical trials of in vitro diagnostics.

Acknowledgements

Appendix A. Supplementary data

Supplementary data associated with this article can be found, in the online version, at doi:10.1016/j.bios.2010.01.039.

References

Almeida, T., Piedade, M., Cardoso, F., Ferreira, H., Freitas, P., 2006. Instrumentation and Measurement Technology Conference. IMTC 2006. Proceedings of the IEEE, 2007–2012.
Baselt, D.R., Lee, G.U., Natesan, M., Metzger, S.W., Sheehan, P.E., Colton, R.J., 1998. Biosensors and Bioelectronics 13, 731–739.
de Boer, B., Kahlman, J., Jansen, T., Duric, H., Veen, J., 2007. Biosensors and Bioelectronics 22, 2366–2370.
Daughton, J., Chen, Y., 1993. IEEE Transactions on Magnetics 29, 2705–2710.
Ferrara, E., Widrow, B., 1981. Acoustics, Speech and Signal Processing, IEEE Transactions on 29, pp. 766–770.
Graham, D.L., Ferreira, H.A., Freitas, P.P., 2004. Trends in Biotechnology 22, 455–462.
Hall, D.A., Gaster, R.S., Osterfeld, S., Wang, S.X., 2009. Temperature and drift compensation in GMR devices. Provisional Patent filed on March 10.
Hall, D.A., Gaster, R.S., Lin, T., Osterfeld, S.J., Han, S., Murmann, B., Wang, S.X., 2010. Biosensors and Bioelectronics 25, 2051–5057.
Han, S., Yu, H., Murmann, B., Pourmand, N., Wang, S.X., 2007. Solid-State Circuits Conference. ISSCC 2007. Digest of Technical Papers. IEEE International, pp. 168–594.
Haykin, S.S., Widrow, B., 2003. Least-Mean-Square Adaptive Filters. Wiley–IEEE.
Lenssen, K.H., Kuiper, A.E.T., van den Broek, J.J., van der Rijt, R.A.F., van Loon, A., 2000. Journal of Applied Physics: AIP, 6665–6667.
Osterfeld, S.J., Yu, H., Gaster, R.S., Caramuta, S., Xu, L., Han, S., Hall, D.A., Wilson, R.J., Sun, S., White, R.L., Davis, R.W., Pourmand, N., Wang, S.X., 2008. Proceedings of the National Academy of Sciences 105, 20637–20640.
Wang, H., Chen, Y., Hassibi, A., Scherer, A., Hajimiri, A., 2009. Solid-State Circuits Conference—Digest of Technical Papers. ISSCC 2009. IEEE International, pp. 438–439, 439a.
Xu, L., Yu, H., Akhras, M.S., Han, S., Osterfeld, S., White, R.L., Pourmand, N., Wang, S.X., 2008. Biosensors and Bioelectronics 24, 99–103.